

Direct observation of dispersive lower Hubbard band in iron-based superconductor FeSe

D. V. Evtushinsky,^{1,*} M. Aichhorn,² Y. Sassa,^{3,4} Z.-H. Liu,¹ J. Maletz,¹ T. Wolf,⁵ A. N. Yaresko,⁶ S. Biermann,⁷ S. V. Borisenko,¹ and B. Büchner^{1,8}

¹*Institute for Solid State Research, IFW Dresden, P. O. Box 270116, D-01171 Dresden, Germany*

²*Institute of Theoretical and Computational Physics, TU Graz, Petersgasse 16, 8010 Graz, Austria*

³*Laboratory for Solid State Physics, ETH Zurich, CH-8093 Zurich, Switzerland*

⁴*Department of Physics and Astronomy, Uppsala University, 751 20 Uppsala, Sweden*

⁵*Karlsruher Institut für Technologie, Institut für Festkörperphysik, 76021 Karlsruhe, Germany*

⁶*Max-Planck-Institute for Solid State Research, Heisenbergstrasse 1, D-70569 Stuttgart, Germany*

⁷*Centre de Physique Theorique, Ecole Polytechnique, CNRS, 91128 Palaiseau Cedex, France*

⁸*Institut für Festkörperphysik, Technische Universität Dresden, D-01171 Dresden, Germany*

Electronic correlations were long suggested not only to be responsible for the complexity of many novel materials, but also to form essential prerequisites for their intriguing properties. Electronic behavior of iron-based superconductors is far from conventional, while the reason for that is not yet understood. Here we present a combined study of the electronic spectrum in the iron-based superconductor FeSe by means of angle-resolved photoemission spectroscopy (ARPES) and dynamical mean field theory (DMFT). Both methods in unison reveal strong deviations of the spectrum from single-electron approximation for the whole $3d$ band of iron: not only the well separated coherent and incoherent parts of the spectral weight are observed, but also a noticeable dispersion of the lower Hubbard band (LHB) is clearly present. This way we demonstrate correlations of the most puzzling intermediate coupling strength in iron superconductors.

Mean field approach to the conduction electrons [1] became a classical theory, and is one of the pillars on which the breakthrough of technology in the 20th century resides. At the same time the potential of the electronic systems, obedient to the pure band theory, seems to be

largely depleted by now. As opposed to the case of negligible correlation effects, the Hubbard model [2] is known to provide a solution in the polar extreme of dominating electronic correlations (see Fig. 1). Interesting properties of many new materials in the scope of the modern condensed matter physics are often found for the regime lying in between normal band metal and correlated insulator [3, 4]. However there is little information as for the actual degree of the electron-electron interaction strength for relevant materials as well as for comprehensive theoretical treatment of the problem.

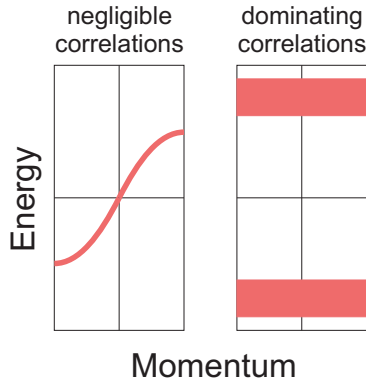


Fig. 1: Schematic representation of the electronic bands without and with correlations. Within mean field approach the electronic spectrum of a crystalline solid consists of bands with well-defined dispersion (left), while in the case of strong electron-electron correlations, Hubbard bands are formed (right).

Electronic correlations were conjectured to be vital for abnormally high critical temperatures in unconventional superconductors [5–9]. In best-known material class, exhibiting highest transition temperatures, — cuprates — the superconductivity rises when additional charge carriers are doped into the antiferromagnetic Mott insulator [10, 11], immediately invoking the suggestion that correlations are relevant. Although many subclasses of iron-based superconductors exhibit a phase diagram very similar to cuprates [12–14], there is no evidence for insulating behaviour at any doping level, questioning the degree of correlation strength and their importance in this case. At the same time various experimental techniques have shown that the electronic states at the Fermi level are renormalized three and more times with respect to the predictions of the local density approximation theory (LDA) [15–20]. Encouragingly similar estimate for band renormalization was obtained in the dynamical mean field theory (DMFT) calculations [21–25]. However, it is still not entirely clear to which extent the underlying physics was captured by DMFT, as renormaliza-

*Current address: BESSY II, Helmholtz-Zentrum Berlin for Materials and Energy, Albert-Einstein-Strasse 15, 12489 Berlin, Germany; Electronic address: danevt@gmail.com

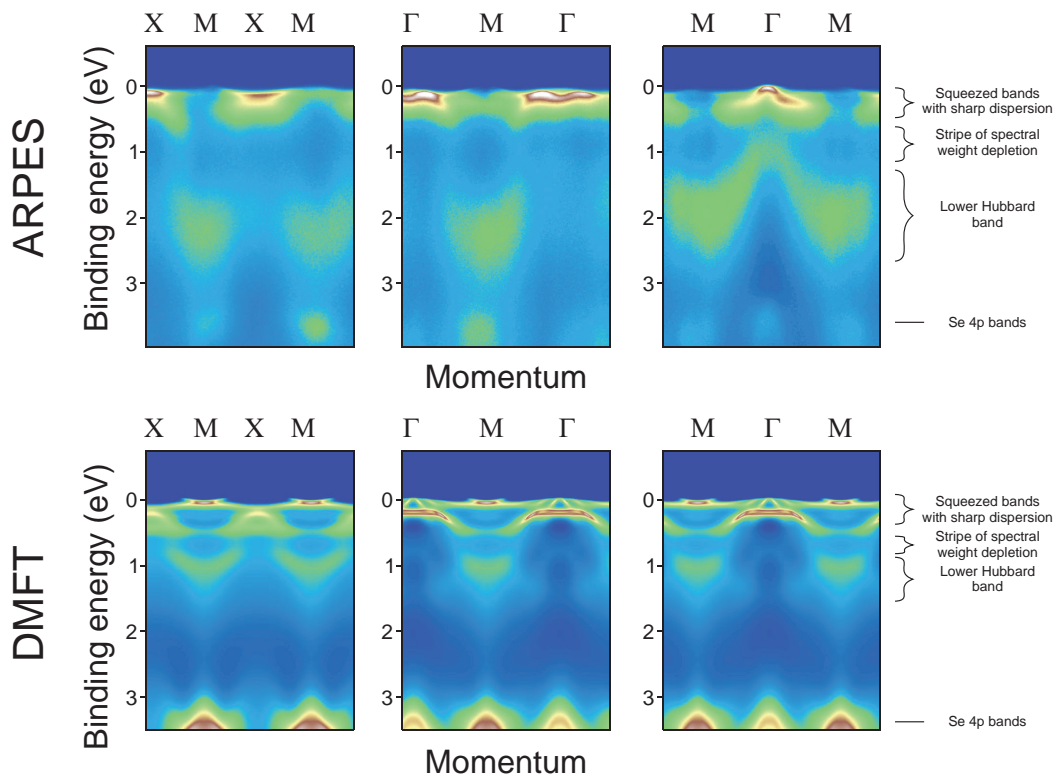


Fig. 2: Electronic spectra of FeSe measured by ARPES and calculated by DMFT. Top row: distribution of the spectral weight for $3d$ band of iron, measured by ARPES along high-symmetry directions in the Brillouin zone. Bottom row: spectral function resulting from DMFT calculations for the same directions. Comparison of DMFT and ARPES shows very good agreement in terms of general structure of the spectrum: In both cases there are squeezed bands with sharp dispersion at the Fermi level, which are separated from the lower Hubbard band by a stripe of spectral weight depletion.

tion of the low-energy spectrum itself is a rather universal effect, and, for example, also encapsulates the contribution from electronic interactions with low-energy bosonic modes.

Here we present angle-resolved photoemission spectroscopy (ARPES) measurements of the electronic spectrum of the simplest iron-based superconductor with potentially highest T_c [26, 27], iron selenide. The experimental spectrum of the iron $3d$ band deviates strongly from the LDA, but exhibits a full-scale match with spectral function obtained by DMFT. Remarkably, along with the sharp Fermi-liquid-like bands at the Fermi level, the well-defined dispersive lower Hubbard band (LHB) is present both in calculated and measured spectrum.

Energy-momentum cuts through the photoemission intensity distribution measured in high symmetry directions for binding energies, ω , up to 4 eV are presented in Fig. 2 along with corresponding plots of the spectral weight distribution obtained in DMFT calculations. Both in ARPES and DMFT the electronic spectrum consists of two parts: (1) renormalized bands with sharp well defined dispersion at the Fermi level and (2) diffuse spectral weight with weak but noticeable dispersion at higher binding energies, with (1) and (2) being separated by a stripe of spectral weight depletion. Such spec-

tral weight distribution is not compatible with single-electron model, while it is common for the solution of the Hubbard model, where (1) is called coherent spectral weight, and (2) is the lower Hubbard band. Details of the photoemission spectrum depend on experimental conditions—photon energy, light polarization, position in the momentum space, as relative photoemission matrix element for different bands can vary in a wide range. Nevertheless, the most prominent and important features persist and match the counterparts in the calculation, implying that DMFT captures all relevant peculiarities of the spectrum. The position of the LHB in the calculated spectral function is subject to the ill-posed analytic continuation problem. In the supplementary material we show how different variants of analytic continuation can change the position of the LHB such that it agrees very well with the experimentally observed one in terms of location and broadening. It is interesting to note that a model for the spectral function with an empirical self-energy of the simplest shape can reproduce the data satisfactorily well [28], however it fails to reproduce the experimentally observed well-defined LHB separated by a sharp stripe of spectral weight depletion, while these features are inherent to the DMFT calculations.

Although the original paper by Hubbard presents Hub-

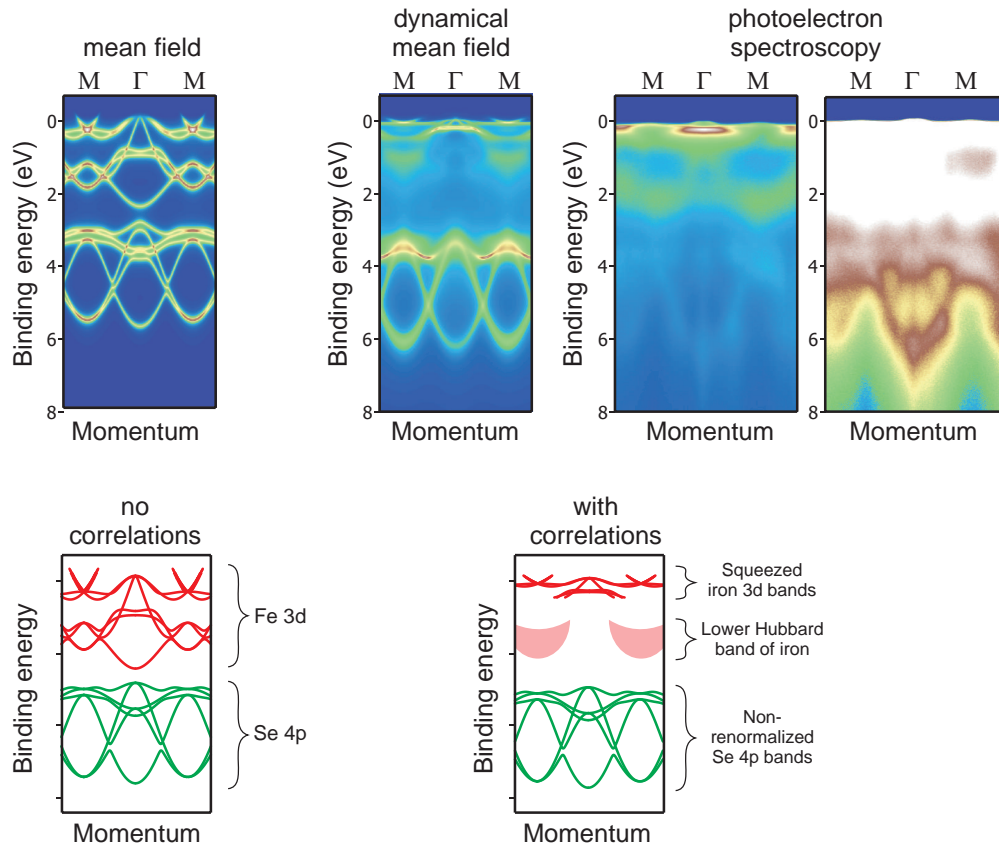


Fig. 3: Spectral function of iron and selenium bands in FeSe as seen by LDA, DMFT and ARPES. Top row: electronic bands obtained in LDA calculations, spectral weight distribution from DMFT and spectra measured by ARPES. The main deviation of the DMFT and ARPES spectra from LDA is separation of iron 3d band into renormalized bands with clear dispersion at the Fermi level and weakly dispersive lower Hubbard band. At the same time selenium 4p bands are renormalized with respect to LDA neither in DMFT nor in ARPES. Bottom row: sketch illustrating structure of the electronic spectrum with and without electronic correlations.

band bands as possessing energy dispersion reminiscent of the unperturbed band [2], commonly they are depicted and thought of as non-dispersive spectral weight. The LHB, that we observe here, indeed exhibits large electron scattering rate and is not sharp. At the same time we do observe appreciable dispersion, equally in ARPES and DMFT: the LHB has minimum and is defined best at the M point, it disperses upwards and loses intensity when departing from the M point in any direction. One of the possible interpretations of the observed picture is that LHB emerges out of the states that would be located at the bottom of the iron band in absence of correlations.

We analysed the orbital content of the lower Hubbard band in the calculated spectrum, and found non-zero contributions from all the orbitals. In particular, also the e_g -like orbitals (z^2 and $x^2 - y^2$), contribute, and their contribution is also located at higher binding energies as compared to the most correlated xy orbitals. This might appear puzzling at first sight, since the e_g orbitals are — thanks to its hybridisation pseudo-gap at the Fermi level — significantly less correlated than the t_{2g} orbitals.

In the supplementary material, we demonstrate that this is not a contradiction: on the contrary, as we show there, the hybridization gap facilitates the detection of the LHB since it pushes the overall feature to lower energies, separating it better from the remaining spectral weight. In contrast, for the xy orbital the Hubbard band is very close to the quasiparticle excitations around the Fermi level and makes it more difficult to separate.

It is instructive to compare spectral functions obtained by LDA, DMFT and ARPES in even wider energy range, encompassing both iron and selenium eV bands. In Fig. 3 we present spectra in the range up to 8 eV of binding energy. Interestingly, the bands, predominantly derived from the selenium orbitals, exhibit little deviation from the LDA calculation, which contrasts the described above behavior of the iron-derived bands. Selenium 4p bands both in ARPES and DMFT are not renormalized with respect to LDA and exhibit moderate electron scattering. Still, one can point out that both in DMFT and in ARPES they are consistently located at a higher binding energy, as compared to the LDA. Very low intensity is explained by

drastically different cross-sections of iron $3d$ and selenium $4p$ shells in the photoemission process; in order to compensate this effect and to make selenium-derived bands better visible, we plot ARPES data in a corresponding color scale (last panel in the top row of Fig. 3). Also refer to the Supplementary Materials for better visualization of the dispersion.

In conclusion, using state-of-the-art ARPES and DMFT, we have provided evidence for a highly dispersive LHB in the — probably most intriguing — representative of iron-based superconductors, FeSe. While the presence of strong Hund's coupling is generally believed to pre-

vent the formation of Hubbard bands, our study reveals a highly dispersive lower Hubbard band, following roughly the non-interacting band dispersion. Our work has implications for other iron-based superconductors, where one may speculate that HBs should be present. It also underlines that the physics of these materials is not only determined by Hund's coupling, but that Coulomb interactions quite generally, and naturally, play a crucial role, too.

Y.S. acknowledges funding from the Wenner-Gren foundation.

-
- [1] F. Bloch, Über die Quantenmechanik der Elektronen in Kristallgittern. *Z. Phys.* **52**, 555 (1928).
- [2] J. Hubbard, Electron Correlations in Narrow Energy Bands. *Proc. R. Soc. Lond. A* **276**, 238 (1963).
- [3] E. Dagotto, Correlated electrons in high-temperature superconductors. *Rev. Mod. Phys.* **66**, 736 (1994).
- [4] M. Imada, A. Fujimori, and Y. Tokura, Metal-insulator transitions. *Rev. Mod. Phys.* **70**, 1039 (1998).
- [5] P. W. Anderson, The Resonating Valence Bond State in La_2CuO_4 and Superconductivity. *Science* **235**, 1196-1198 (1987).
- [6] T. A. Maier, M. Jarrell, T. C. Schulthess, P. R. C. Kent, and J. B. White, Systematic Study of d-Wave Superconductivity in the 2D Repulsive Hubbard Model. *Phys. Rev. Lett.* **95**, 237001 (2005).
- [7] K. Haule and G. Kotliar, Strongly correlated superconductivity: A plaquette dynamical mean-field theory study. *Phys. Rev. B* **76**, 104509 (2007).
- [8] D. J. Scalapino, A common thread: The pairing interaction for unconventional superconductors. *Rev. Mod. Phys.* **84**, 1383 (2012).
- [9] S. Raghu, E. Berg, A. V. Chubukov, and S. A. Kivelson, Effects of longer-range interactions on unconventional superconductivity. *Phys. Rev. B* **85**, 024516 (2012).
- [10] T. Fujita, Y. Aoki, Y. Maeno, J. Sakurai, H. Fukuba and H. Fujii, Crystallographic, Magnetic, and Superconductive Transitions in $(\text{La}_{1-x}\text{Ba}_x)_2\text{CuO}_{4-y}$, *Jpn. J. Appl. Phys.* **26** L368 (1987).
- [11] P. A. Lee, N. Nagaosa, and X.-G. Wen, Doping a Mott insulator: Physics of high-temperature superconductivity. *Rev. Mod. Phys.* **78**, 17 (2006).
- [12] Y. Kamihara, T. Watanabe, M. Hirano, H. Hosono, *J. Am. Chem. Soc.* **11**, 3296 (2008).
- [13] G. R. Stewart, *Rev. Mod. Phys.* **83**, 1589 (2011).
- [14] Johnpierre Paglione and Richard L. Greene, *Nat. Phys.* **6**, 645 (2010).
- [15] P. Popovich, A. V. Boris, O. V. Dolgov, A. A. Golubov, D. L. Sun, C. T. Lin, R. K. Kremer, and B. Keimer, Specific Heat Measurements of $\text{Ba}_{0.68}\text{K}_{0.32}\text{Fe}_2\text{As}_2$ Single Crystals: Evidence for a Multiband Strong-Coupling Superconducting State. *Phys. Rev. Lett.* **105**, 027003 (2010).
- [16] S. V. Borisenko, V. B. Zabolotnyy, D. V. Evtushinsky, T. K. Kim, I. V. Morozov, A. N. Yaresko, A. A. Kordyuk, G. Behr, A. Vasiliev, R. Follath, and B. Büchner, Superconductivity without Nesting in LiFeAs . *Phys. Rev. Lett.* **105**, 067002 (2010).
- [17] S. T. Cui, S. Y. Zhu, A. F. Wang, S. Kong, S. L. Ju, X. G. Luo, X. H. Chen, G. B. Zhang, and Z. Sun, Evolution of the band structure of superconducting NaFeAs from optimally doped to heavily overdoped Co substitution using angle-resolved photoemission spectroscopy. *Phys. Rev. B* **86**, 155143 (2012).
- [18] D. V. Evtushinsky, V. B. Zabolotnyy, T. K. Kim, A. A. Kordyuk, A. N. Yaresko, J. Maletz, S. Aswartham, S. Wurmehl, A. V. Boris, D. L. Sun, C. T. Lin, B. Shen, H. H. Wen, A. Varykhalov, R. Follath, B. Büchner, and S. V. Borisenko, Strong electron pairing at the iron $3d_{xz,yz}$ orbitals in hole-doped BaFe_2As_2 superconductors revealed by angle-resolved photoemission spectroscopy. *Phys. Rev. B* **89**, 064514 (2014).
- [19] Taichi Terashima, Motoi Kimata, Nobuyuki Kurita, Hidetaka Satsukawa, Atsushi Harada, Kaori Hazama, Motoharu Imai, Akira Sato, Kunihiko Kihou, Chul-Ho Lee, Hijiri Kito, Hiroshi Eisaki, Akira Iyo, Taku Saito, Hideto Fukazawa, Yoh Kohori, Hisatomo Harima, Shinya Uji, Fermi surface and mass enhancement in KFe_2As_2 from de Haas-van Alphen effect measurements. *J. Phys. Soc. Jpn.* **79**, 053702 (2010).
- [20] J. Maletz, V. B. Zabolotnyy, D. V. Evtushinsky, S. Thirupathiah, A. U. B. Wolter, L. Harnagea, A. N. Yaresko, A. N. Vasiliev, D. A. Chareev, A. E. Böhmer, F. Hardy, T. Wolf, C. Meingast, E. D. L. Rienks, B. Büchner, and S. V. Borisenko, Unusual band renormalization in the simplest iron-based superconductor FeSe_{1-x} . *Phys. Rev. B* **89**, 220506(R) (2014).
- [21] I. A. Nekrasov, N. S. Pavlov, M. V. Sadovskii, LDA'+DMFT Investigation of Electronic Structure of $\text{K}_{1-x}\text{Fe}_{2-y}\text{Se}_2$ Superconductor. *JETP Letters* **97**, 15 (2013).
- [22] M. Aichhorn, L. Pourovskii, V. Vildosola, M. Ferrero, O. Parcollet, T. Miyake, A. Georges, S. Biermann, Dynamical mean-field theory within an augmented plane-wave framework: Assessing electronic correlations in the iron pnictide LaFeAsO . *Phys. Rev. B* **80**, 085101 (2009).
- [23] J. Ferber, K. Foyevtsova, R. Valenti, and H. O. Jeschke, LDA + DMFT study of the effects of correlation in LiFeAs . *Phys. Rev. B* **85**, 094505 (2012).
- [24] Z. P. Yin, K. Haule, G. Kotliar, Kinetic frustration and the nature of the magnetic and paramagnetic states in iron pnictides and iron chalcogenides. *Nature Materials* **10**, 932 (2011).
- [25] M. Aichhorn, S. Biermann, T. Miyake, A. Georges, and

- M. Imada, Theoretical evidence for strong correlations and incoherent metallic state in FeSe. *Phys. Rev. B* **82**, 064504 (2010).
- [26] Jian-Feng Ge, Zhi-Long Liu, Canhua Liu, Chun-Lei Gao, Dong Qian, Qi-Kun Xue, Ying Liu, and Jin-Feng Jia, Superconductivity above 100 K in single-layer FeSe films on doped SrTiO₃. *Nature Materials* **14**, 285 (2015).
- [27] Shiyong Tan, Yan Zhang, Miao Xia, Zirong Ye, Fei Chen, Xin Xie, Rui Peng, Difei Xu, Qin Fan, Haichao Xu, Juan Jiang, Tong Zhang, Xinchun Lai, Tao Xiang, Jiangping Hu, Binping Xie, and Donglai Feng, Interface-induced superconductivity and strain-dependent spin density waves in FeSe/SrTiO₃ thin films. *Nature Materials* **12**, 634 (2013).
- [28] D. V. Evtushinsky, A. N. Yaresko, V. B. Zabolotnyy, J. Maletz, T. K. Kim, A. A. Kordyuk, M. S. Viazovska, M. Roslova, I. Morozov, R. Beck, S. Wurmehl, H. Berger, B. Büchner, and S. V. Borisenko, Anomalous High-Energy Electronic Interaction in Iron-Based Superconductor. In preparation.

Supplementary materials

I. FERMI SURFACE MAP AND SUPERCONDUCTING TRANSITION IN ARPES OF FESE

In Fig. S1 one can see ARPES data recorded from freshly cleaved surface of single crystalline sample of FeSe. A Fermi surface (FS) map and a temperature dependence of the integrated energy distribution curve confirming superconducting transition in the studied matter are presented. The Fermi surface consists of hole-like pocket at the Brillouin zone (BZ) center, Γ point, and of electron-like pocket at the BZ corner, M point. In the region of low binding energies the electronic bands, supporting the Fermi surface, are very reminiscent of the ones obtained in LDA. The major difference is that experimentally observed bands are renormalized by factor of three and more with respect to the calculation. Temperature-dependent measurements reveal the growth of the well-defined coherence peak, showing the opening of the superconducting gap below transition temperature of about 8 K.

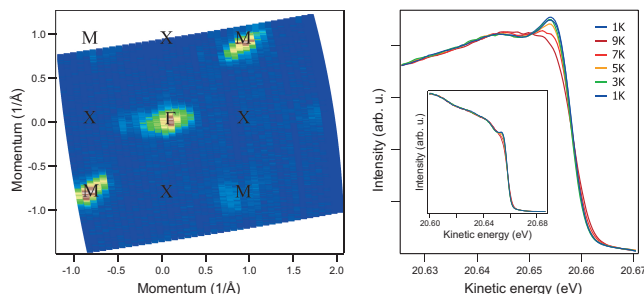


Fig. S 1: Fermi surface map and observation of the superconducting transition in ARPES spectra of single crystals of FeSe. Left: distribution of photoemission intensity at the Fermi level recorded at photon energy of 80 eV confirms hole-like Fermi surface sheets around the Γ point and electron-like ones at the M point. Right: temperature dependence of the partial density of states referring to the Γ pocket reveals growth of the coherence peak below T_c of about 8 K. Spectra in a wider energy range are shown in the inset.

II. DISPERSION OF SE 4P BANDS FROM ARPES

Observation of the clear dispersion of the 4p bands of selenium (Fig. S2) in ARPES data ensures generally good agreement with band structure calculation in a wide range of binding energy, from 0 up to 8 eV. Selenium bands reveal sharp dispersion, relatively small scattering rate, and virtually no renormalization with respect

to the LDA calculations. At the same time an interesting observation regarding the difference between LDA and ARPES can be made: the experimental 4p bands are shifted towards higher binding energies by about 1 eV, as compared to the band theory. A similar shift of 4p can be observed when DMFT results are matched with LDA, see Fig. 3 of the main text. In the Fig. S2 the color scale is set in a way visualizing the dispersion of the 4p bands the best. Photoemission matrix elements vary in a wide range upon changing the experimental conditions, and different parts of the band appear intense and suppressed depending on the photon energy and polarization, and on the electron emission angle. In the panel (a) the results of the LDA calculation are presented, while in the panel (e) only the 4p band, shifted to the experimentally observed position, is shown.

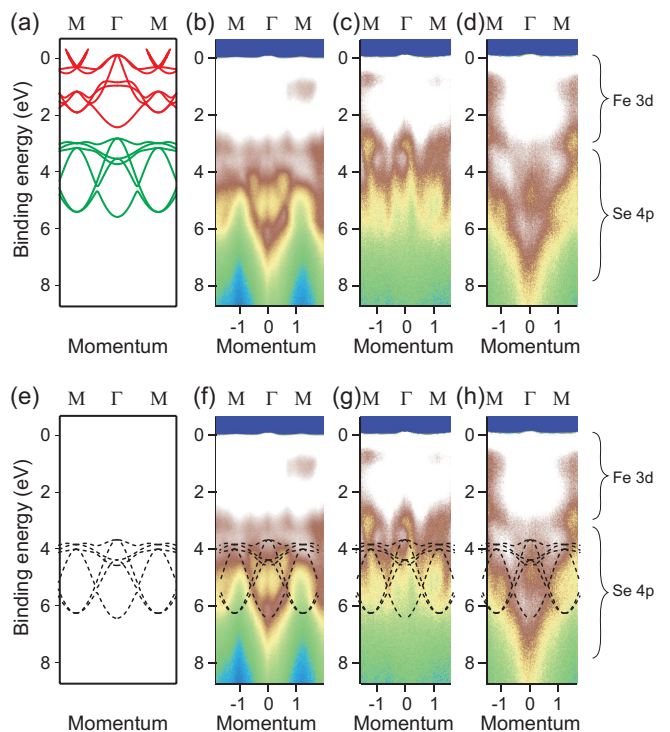


Fig. S 2: Dispersion for the selenium-derived bands in FeSe. (a) Band dispersion from LDA calculations. (b,c,d) Spectra of FeSe along M Γ M direction measured with different photon energies and light polarization in order to highlight different parts of the Se 4p band. (e) Position of Se bands corresponding to the one observed experimentally. (f,g,h) same as (b,c,d) with superimposed contours of Se bands.

III. INDEPENDENCE OF LOWER HUBBARD BAND POSITION IN ARPES AS A FUNCTION OF PHOTON ENERGY

Photoemission matrix elements can have a strong impact on the measured signal, especially when the spectral

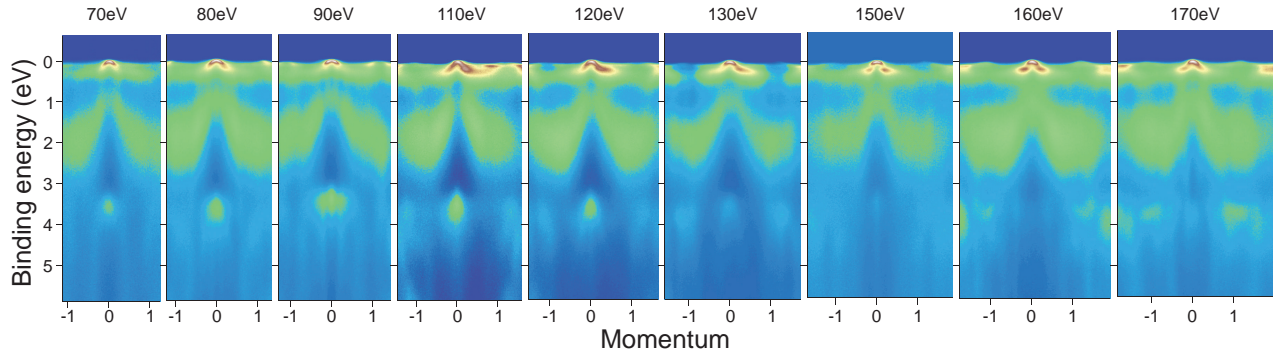


Fig. S 3: An energy-momentum cut passing through the Γ point, recorded at various photon energies and vertical light polarization. The photon energies are indicated above the corresponding intensity plots. One can see that the distribution of photoemission intensity in the region of binding energies 0.5..3 eV, where the LHB resides, is rather universal, implying that although the matrix elements play important role, one can extract the parameters of the LHB from experiment with good precision.

function consists of rather broad peaks. In order to reveal the true underlying distribution of the spectral weight, we have performed measurements at different conditions. A series of spectral images, recorded along the direction passing through the Brillouin zone center, the Γ point, at different photon energies, are presented in the Fig. S3. The generic features of the spectral weight distribution, such as positions of the coherent spectral weight, LHB, a stripe of the spectral weight depletion between them remain unchanged.

IV. LOWER HUBBARD BAND POSITION IN DMFT

In the main text of this paper we included DMFT data that is produced in accordance with Ref. S1, in order to be consistent with published data. We use a continuous time quantum Monte Carlo technique [S2] for the calculations, which produces Greens functions and self energies on the Matsubara frequency axis. In order to get data on the real-frequency axis that can be compared to the ARPES experiments, one faces the ill-posed analytic continuation (AC) problem. In addition, the AC is not defined to be used directly for self energy. For the data in the main text—and also in Ref. S1—we used the following procedure. One defines an artificial Greens function, $\tilde{G}(i\omega) = \frac{1}{i\omega - \Sigma(i\omega) + \Sigma^{\text{DC}}}$, where Σ^{DC} is the double counting correction. This $\tilde{G}(i\omega)$ is continued to the real frequency axis, which after inversion of above equation leads to the real frequency $\Sigma(\omega)$. Since $\Sigma(i\omega)$ is damped by the $1/i\omega$ tail of the Greens function, high energy features of $\Sigma(\omega)$ are particularly smooth.

Here, we analyse the influence of this smoothing by applying another scheme to do the analytic continuation of the self energy. We modify $\Sigma(i\omega)$ directly, such that it behaves as a Greens function. In other words, we define the artificial function $\tilde{\Sigma}(i\omega)$ by subtracting the real

part of $\Sigma(i\omega \rightarrow \infty)$, and rescaling it such that $\tilde{\Sigma}(i\omega)$ is normalised to one. Then, one can apply AC directly to $\tilde{\Sigma}(i\omega)$.

In Fig. S4 we compare the two methods, using the artificial Greens function $\tilde{G}(i\omega)$, left (a), and the rescaled self energy, right (b). It is immediately obvious that the overall features—low energy renormalization, spectral weight suppression, lower Hubbard bands—are similar in both methods. The position and sharpness of the features, however, differ between the methods, in particular at high energies. This is not surprising, given the ill-posedness of the AC. Using the rescaled self energy puts the position of the Hubbard bands even closer to what is measured in ARPES. Nevertheless, in order to be consistent with published data, we discuss both variants of

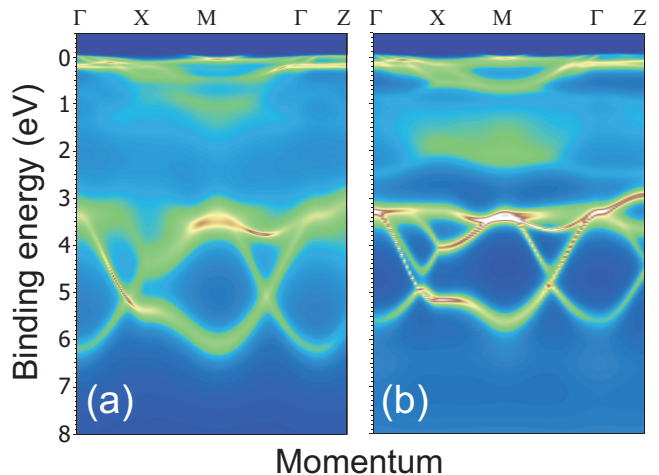


Fig. S 4: Calculated spectral function using two different variants of the analytic continuation method for the self energy. Left (a) using an artificial Greens function, right (b) using a rescaling of the self energy.

doing the AC, and do not just use one of them.

V. INFLUENCE OF THE ONE-PARTICLE BAND STRUCTURE ON THE DISPERSION OF HUBBARD BANDS: SPECTRAL PROPERTIES OF CORRELATED ORBITALS WITH HYBRIDISATION GAP

In this section, we show why the existence of a single-particle pseudogap in the non-interacting density of states in a multi-orbital system helps the formation of Hubbard bands in those orbitals. The mechanism is simple: the separation of the Hubbard bands, which in the atomic limit is given by the Hubbard U (for simplicity we consider a model with $J=0$), is substantially enhanced by the hybridization, see Fig. S5, and equations below.

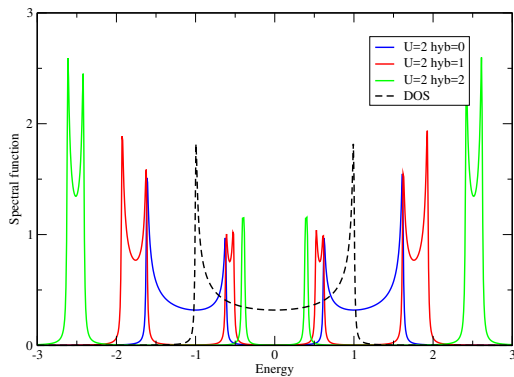


Fig. S 5: Spectral function of a two-orbital model with non-interacting DOS given by the dashed black lines, calculated within the Hubbard 1 approximation.

Let's consider a Hubbard model with two orbitals with Hamiltonian given by $H_{11} = \epsilon_k = -H_{22}$, $H_{12} = v$. For the application below, we will take ϵ_k in the form of a cosine band, but this is not essential, as long as the two

bands ϵ_k and $-\epsilon_k$ intersect. The effect of v is then obviously to open a hybridisation gap.

The eigenvalues are

$$E_{\pm}^{(0)} = \pm\sqrt{\epsilon_k^2 + v^2} \quad (1)$$

Now, we add Hubbard interactions **on the original orbitals**. We use the Hubbard 1 approximation, that is, we assume the self-energy not to be modified by the hopping:

$$\Sigma(\omega + i\eta) = \frac{U^2}{4(\omega + i\eta)^2} \quad (2)$$

This splits each of the two bands, and the spectral function consists of poles at energies

$$E_{\pm} = \pm\frac{1}{2}E_{\pm}^{(0)} \pm \frac{1}{2}\sqrt{(E_{\pm}^{(0)})^2 + U^2} \quad (3)$$

$$= \pm\frac{1}{2}\sqrt{\epsilon_k^2 + v^2} \pm \frac{1}{2}\sqrt{\epsilon_k^2 + v^2 + U^2} \quad (4)$$

The two outermost features (Hubbard bands) are separated by

$$\sqrt{\epsilon_k^2 + v^2} + \sqrt{\epsilon_k^2 + v^2 + U^2} \quad (5)$$

which exceeds both, the non-interacting bonding-antibonding splitting of $2\sqrt{\epsilon_k^2 + v^2}$ and the Hubbard splitting in the absence of hopping/hybridisation U . The effect of the hybridisation gap is thus to push the Hubbard features away from the Fermi level, making them easier to detect. The dispersion of the lower Hubbard bands is then essentially given by the dispersion of the non-interacting band, shifted to higher binding energies.

This explains why Hubbard bands in iron-based superconductor materials are most prone to appear in those bands that are “pseudo-gapped” (at the single particle level), resolving the apparent contradiction of the Hubbard band having substantial weight on the least correlated orbitals.

[S1] M. Aichhorn, S. Biermann, T. Miyake, A. Georges, and M. Imada, Theoretical evidence for strong correlations and incoherent metallic state in FeSe. *Phys. Rev. B* **82**, 064504 (2010).

[S2] P. Seth *et al.*, TRIQS/CTHYB: A continuous-time quan-

tum Monte Carlo hybridisation expansion solver for quantum impurity problems, *Computer Physics Communications* **200**, 274 (2015).